Catalysis Today xxx (xxxx) xxx–xxx

Contents lists available at ScienceDirect

Catalysis Today

journal homepage: www.elsevier.com/locate/cattod

# Synergistic catalysis of hybrid nano-structure Pd catalyst for highly efficient catalytic selective hydrogenation of benzaldehyde

Yanji Zhang[a,b], Jicheng Zhou[a,b,*], Kai Li[a,b], Mengdie Lv[a,b]

[a] Key Laboratory of Green Catalysis and Chemical Reaction Engineering of Hunan Province, Xiangtan, 411105, Hunan Province, China
[b] School of Chemical Engineering, Xiangtan University, Xiangtan, 411105, Hunan Province, China

ARTICLE INFO

*Keywords:*
Synergistic catalysis
Hybrid nano-structure catalyst
Benzaldehyde hydrogenation
Photochemical route
Selective hydrogenation

ABSTRACT

Selective hydrogenation of benzaldehyde is a green and sustainable technology to produce benzyl alcohol. Herein, we report a hybrid nano-structure catalyst(Pd/@-$ZrO_2$/AC) by photochemical route for selective hydrogenation of benzaldehyde under mild reaction conditions. The Pd/@-$ZrO_2$/AC catalyst exhibited outstanding activity(100%) and high selectivity for benzyl alcohol (> 98 %), much higher than that of Pd/$ZrO_2$ and Pd/AC. The high catalytic activity was attributed to the special structure and the synergistic effect. A series of Pd/@-$Me_xO_y$/AC($Me_xO_y$: $TiO_2$, $CeO_2$, $La_2O_3$) catalysts further confirmed the synergistic effect in this hybrid nano-structure for this reaction. This work clearly demonstrates that loading nano-metal on high specific surface area materials with nano-semiconductors can increase the catalytic activity and open up a new direction for the synergistic catalysis of hybrid nano-structure catalysts.

## 1. Introduction

Benzyl alcohol is an important intermediate in the synthesis of a wide variety of esters, which is used in vitamins, pharmaceuticals, pesticides, flavor, fragrances, and various esters [1–4]. Previously, the conventional synthetic method for obtaining the corresponding alcohol was to hydrolyze benzyl chloride using sodium hydroxide, but this reaction released chlorine produced significant by-products (benzyl ether and NaCl), which were harmful to the application and caused serious environmental toxicity [5]. Recently, it has been found that the selective hydrogenation of benzaldehyde to benzyl alcohol is a better choice [6–8]. However, it is still a challenge to avoid further hydrodeoxygenation of benzyl alcohol into toluene. The preparation pathways are shown in Scheme 1.

Various metal catalysts such as Ni [9–11], Cu [12], Co [13], Pt [11,14–17], Au [5,18,19], Ru [20–22] and Pd [3,7,8,11,23–27] were used for the hydrogenation of benzaldehyde to benzyl alcohol. Palladium was the most widely used catalyst, but it was a challenge to achieve satisfactory selectivity of benzyl alcohol when benzaldehyde was completely reacted under mild conditions. Therefore, increasing the activity of palladium catalysts while maintaining their high selectivity has become an urgent task for further development in this field. In the hydrogenation of aromatic ring compounds, the activation of hydrogen is an important step. Many factors play an important role in this reaction, such as properties of support, metal-support interaction, crystallite size of metals and so on. The choice of appropriate support can have a significant effect on both the activity and selectivity in certain reactions. Various researchers compared the activity of Pd with different supports. The most commonly used supports were carbon material and metal oxide. Xinhe Bao et al. [24] studied the selectivity of benzyl alcohol by using the functionalization of carbon nanotubes (CNTs) as the support of Pd. The introduction of oxygen-containing groups in the CNTs reduced the selectivity to the intermediate benzyl alcohol (27 %), whereas doping with N atoms significantly inhibited the further hydrogenation of benzyl alcohol and thus increased its selectivity (96 %). GeonJoong Kim et al. [25] prepared Pd/carbon nanotubes (CNTs), Pd/r-$Al_2O_3$ and Pd/$SiO_2$ catalysts. The order of selectivity to benzyl alcohol was Pd/CNT (4.7 %) < Pd/$SiO_2$ (88.4 %) < Pd/γ-$Al_2O_3$ (92.9 %), and the corresponding benzaldehyde conversion was Pd/γ-$Al_2O_3$ (15.5%) < Pd/$SiO_2$ (70.3%) < Pd/CNTs (1.0%). Carmine Capacchione et al. [26] compared the activity of Pd/mayenite($Ca_{12}Al_{14}O_{33}$) and Pd/C catalysts, because of the presence of hydride species on the $Ca_{12}Al_{14}O_{33}$, the catalytic performance of Pd/$Ca_{12}Al_{14}O_{33}$ was superior in terms of selectivity at 120℃ (91 % conversion and 99 % selectivity to benzyl alcohol within 5 h). But low catalyst activity of Pd/$Ca_{12}Al_{14}O_{33}$ at room temperature (68 % conversion and 99 % selectivity to benzyl alcohol within 5 h). Masaki Okamoto et al. [27] reported the use of polyethylene glycol (PEG) as a

* Corresponding author at: School of Chemical Engineering, Xiangtan University, Xiangtan, 411105, Hunan Province, China.
*E-mail addresses:* zhoujicheng2012@126.com, zhoujicheng@sohu.com (J. Zhou).

https://doi.org/10.1016/j.cattod.2020.01.022
Received 5 March 2019; Received in revised form 16 October 2019; Accepted 19 January 2020

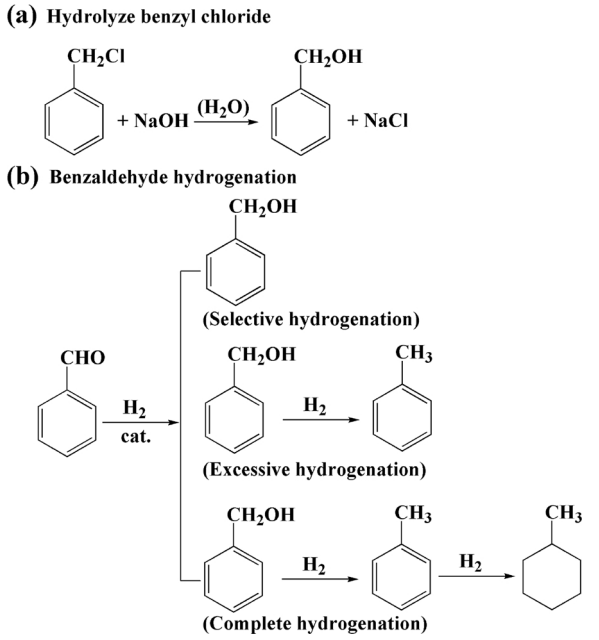


**Scheme 1.** The preparation pathways of benzyl alcohol by hydrolyze benzyl chloride(a) and benzaldehyde hydrogenation(b).

modifiers for $Pd/SiO_2$ catalyst in the hydrogenation of benzaldehyde, oxygen of PEG was coordinated to palladium atoms on the surface, and possibly repulsion between benzyl alcohol and the electron-rich palladium on the surface leads to inhibit further hydrogenation to form toluene, thus increased the selectivity of benzyl alcohol. Although the selectivity of benzyl alcohol was achieved 100%, the highest benzaldehyde conversion was 84 % in liquid-phase hydrogenation. Therefore, circumventing hydrogenolysis and phenyl ring reduction at high conversion remains challenging in the hydrogenation of benzaldehyde to benzyl alcohol [28,29].

In our previous work [30,31], we investigated the catalytic performances of $Pd/@\text{-}Me_xO_y/AC$(Me: Ti, Ce, La) for the hydrogenation of phenol, we found that this Pd catalyst exhibited synergistic interactions between the Pd nanoparticles and metal oxide. In this work, we prepared a hybrid nano-structure $Pd/@\text{-}ZrO_2/AC$ catalyst. The Pd nanoparticles were anchored on the activated carbon (AC) which has a nano-semiconductor layer. This $Pd/@\text{-}ZrO_2/AC$ catalyst exhibited strong synergistic catalysis and showed excellent activity in the hydrogenation of benzaldehyde to benzyl alcohol, much higher than that of $Pd/ZrO_2$ and Pd/AC.

## 2. Experimental

### 2.1. Catalyst preparation

The chemicals, if unspecified, were of analytical grade (A.R.) and purchased from Tianjin Ke Miou Chemical Reagent Co., Ltd. The gases were purchased from Xiangtan Gas Co., Ltd.

Pretreatment of activated carbon with acid. A commercial activated carbon (AC) made from coconut shells (Fujian Xinsen Carbon Co. Ltd.) was pretreated with $HNO_3$ (10 %) under refluxing at 60℃ for 2 h. Then the AC was cooled to room temperature, washed to neutrality with deionized water. Finally, the AC was dried at 120℃.

Preparation of $ZrO_2/AC$. $ZrOCl_2{\cdot}8H_2O$(1.453 g) dissolved in deionized water(50 mL), while stirring, add the pre-processed AC(5 g) in it, 1.5 mol/L $NH_3{\cdot}H_2O$ was added dropwise until the pH of the resulting solution was 10, the mixture was vigorously stirred during the addition, after aging for 24 h, the precipitate was filtered and washed several times by deionized water, and then dried at 100℃ followed by calcination at 500℃ for 4 h. The preparation of $ZrO_2/CNTs$ was the same as above, the only difference was to $ZrO_2/AC$ with $ZrO_2/CNTs$.

Preparation of $TiO_2/AC$. 3 g tetrabutyl titanate was first dissolved in 25 mL ethanol by stirring and then 1.3 mL acetic acid was added into the mixture to obtain solution A. A solution of 15 mL ethanol and 1.5 mL distilled water was denoted by solution B. Then solution B was added into solution A dropwise under vigorous stirring to form sol C. Subsequently, the pretreatment AC was dispersed into sol C and nitric acid was used to adjust pH to 3. After being treated by ultrasonic agitation, the mixture was left at ambient temperature to form the gel. The obtained material was dried at 80℃ for 12 h, and then calcined at 550℃ for 2 h.

Preparation of $CeO_2/AC$. $Ce(NO_3)_3{\cdot}6H_2O$(1.46 g) dissolved in ethanol(120 mL), while stirring, add the pre-processed AC(5 g) in it, 1 mol/L NaOH was added dropwise until the pH of the resulting solution was 10, put the solution in the microwave with the power was set 214 W for 10 min(on for 10 s, off for 20 s). After cooled down to room temperature, washed with distilled water and ethanol then left to dry at 120℃ for 12 h.

Preparation of $La_2O_3/AC$. In a typical synthesis, $La(NO_3)_2{\cdot}nH_2O$ (0.554 g) dissolved in distilled water(120 mL), while stirring, add the pre-processed AC(5 g) in it, 0.5 mol/L $NH_4HCO_3$ was added dropwise until the pH of the resulting solution was 7.0, put the solution in the microwave with the power was set 400 W for 16 min(on for 30 s, off for 30 s). After filtrating, washing and dry at 70℃ for 4 h, finally achieved composite support $La_2O_3/AC$ after calcined at 550℃ for 2 h.

According to principles of the spontaneous monolayer distribution [32], when the content of metal oxide is less than a certain threshold and surface area of the support is large enough, metal oxide would disperse on the support at the state of the spontaneous monolayer distribution, so an appropriate amount of metal oxide can form a single or multi-layer nano-semiconductor layer on AC(CNTs).

The preparation of metal oxide was the same as above, just not add the AC.

Preparation of $Pd/@\text{-}ZrO_2/AC$. It was adapted from the method of our previous work [30,31]. As-prepared $ZrO_2/AC$(0.475 g) was added in deionized water(100 mL) and methanol(3 mL) mix solution, added the $H_2PdCl_4$(0.4 mL, 0.012 g/mL) in it, ultrasonic dispersion for 30 min, then ultraviolet lamp(220/15 W, Guangzhou Cnlight Optoelectronics Technology Co., Ltd.) for 10 h. Finally, the sample was separated by filtration, washed several times by distilled water up to pH = 7, dried in a vacuum oven at 80℃ for 10 h. The preparation of $Pd/@\text{-}La_2O_3/AC$, $Pd/@\text{-}CeO_2/AC$, $Pd/@\text{-}TiO_2/AC$, $Pd/@\text{-}ZrO_2/CNTs$, $Pd/@\text{-}TiO_2$, $Pd/CeO_2$, and $Pd/La_2O_3$ were the same as above, the only difference was to $ZrO_2/AC$ with different supports.

Synthesis of Pd/AC or Pd/CNTs. Because the AC could not be excited and then generate electrons($e^-$) and holes($h^+$) under the UV irradiation, so the Pd/AC or Pd/CNTs were prepared by liquid-phase reduction. AC or CNTs was impregnated with an ethylene glycol solution containing $H_2PdCl_4$ and hydrazine hydrate, stirred at 80℃ for 4 h. Then washed several times by distilled water and ethanol, dried in a vacuum oven at 80℃ for 10 h.

### 2.2. Catalyst characterization

X-ray diffraction (XRD) of samples was obtained on a Rigaku D/max-II/2500 X-ray powder diffractometer, Cu Kα radiation was employed and the working voltage and current were 40 kV and 30 mA, respectively. Transmission electron microscope(TEM) images were obtained with a JEOL JEM-2100 F at an acceleration voltage of 200 kV. X-ray photoelectron spectroscopy (XPS) was performing using ESCALAB 250Xi (Thermo) with Al Kα radiation. The specific surface areas of the samples were calculated by the BET method by $N_2$ adsorption-desorption with a NOVA-2200e volumetric adsorption analyzer. Temperature-programmed reduction by hydrogen ($H_2$-TPR) was carried out on Chem Bet 3000 analyzer. All samples (0.1 g) were pretreated in

the flow of Ar at 250℃ for 1 h. Inductively coupled plasma-atomic emission spectrometry (ICP-AES) data were obtained using an IntrepidII XSP (IRIS). Thermal Gravity Analysis (TGA) was performed on a TGA/DSC1/1600 H T under a nitrogen atmosphere.

### 2.3. Catalyst tests

The typical procedure for hydrogenation of benzaldehyde was as follows: 0.05 g catalyst, 1.88 mmol benzaldehyde, and 20 mL solvent were placed in an autoclave. The autoclave was purged with $H_2$ to remove the air 3 times. Then the reaction was stirred at 800 rpm under 0.7 MPa $H_2$ pressure until the temperature reached reaction temperature. After the end of the reaction, the autoclave was cooled to room temperature, then analyzed using an Agilent 6890 N GC with an HP-5 (30m*0.32mm*0.25 μm) capillary column and FID detector. The temperature of gasify room and detector were 250℃ and 280℃ respectively. The air at a constant flow of 400 mL/min, the mixed gas $H_2$ and $N_2$ flow of 30 mL/min. The initial column temperature was fixed at 70℃ for 1 min and then increased to 210℃ at a rate of 20℃/min. The final temperature was maintained for 3 min. The conversion and selectivity were calculated as follows:

Conversion of benzaldehyde(%) = (Moles of benzaldehyde converted)/(Moles of benzaldehyde initially) × 100%.0 %

Selectivity of benzyl alcohol(%) = (Moles of benzyl alcohol)/(Moles of benzaldehyde converted) × 100%.0 %

## 3. Results and discussion

### 3.1. Characterization

The relevant physicochemical parameters of the Pd/@-$ZrO_2$/AC catalyst were shown in Fig. 1. From Fig. 1(a), the $ZrO_2$/AC and Pd/@-$ZrO_2$/AC samples displayed the typical diffraction peaks at 2Θ = 30.2°, 35.0°, 50.4° and 60.0°, which were readily assigned to tetragonal $ZrO_2$(t-$ZrO_2$)(JCPD 03-0640), the peaks at 2Θ of 27.9° was assigned to monoclinic $ZrO_2$(m-$ZrO_2$)(JCPD 01-0750). For Pd/@-$ZrO_2$/AC, the characteristic diffraction peaks at 2Θ = 40.2° and 46.6° corresponding to (111) and (200) crystalline planes of Pd(JCPD 65–2867).

The TPR profiles were compiled in Fig. 1(b). The $H_2$ consumption peaks at low and high reduction temperatures were assigned to the reduction of PdO having a weak and strong interaction with $ZrO_2$ support [33]. For Pd/@-$ZrO_2$/AC, the reduction peaks of PdO at above 183℃, but the reduction temperature of individual PdO was 50℃ [34]. It was demonstrated that the hybrid nano-structure catalyst exhibited an interaction between nano-Pd and nano-$ZrO_2$/AC. Zheng et al. [33] studied $H_2$-TPR of Pd/$ZrO_2$ which obtained different calcination temperatures of $ZrO_2$(300, 500 and 600℃). They concluded that the intensity of $H_2$ consumption peak of Pd/$ZrO_2$-500 at high reduction temperature(~110℃) was higher than that of Pd/$ZrO_2$-300(~95℃) and Pd/$ZrO_2$-600(~100℃). Pd/$ZrO_2$-500 exhibited a relatively high strong metal-support interaction than other catalysts. Compared with Pd/$ZrO_2$-500, a shift towards higher temperature(183℃) was visualized by Pd/@-$ZrO_2$/AC($ZrO_2$/AC calcined at 500℃), which exhibited stronger metal-support interaction of Pd/@-$ZrO_2$/AC than that of Pd/$ZrO_2$-500.

The $N_2$ adsorption and desorption isotherms of Pd/@-$ZrO_2$/AC and $ZrO_2$/AC were shown in Fig. 1(c), and these two samples displayed type IV isotherms. Accordingly, the BET specific surface areas of AC, $ZrO_2$/AC, and Pd/@-$ZrO_2$/AC were 1419 $m^2$/g, 1183 $m^2$/g, and 1162 $m^2$/g, respectively.

Fig. 1(d–f) showed the survey XPS spectrum and Pd 3d, Zr 3d spectra of the Pd/@-$ZrO_2$/AC catalyst. From Fig. 1(d), Pd, Zr, C, O was detected in the sample. In Fig. 1(e), two signals were observed at values of binding energy around 335.1 eV and 341.1 eV, which could be assigned to the formation of traces of Pd $3d_{5/2}$ and Pd $3d_{3/2}$, respectively [35]. The measured values were slightly different from the standard values(335 eV and 340.3 eV), indicated that there was a strong metal-support interaction between nano-Pd and nano-$ZrO_2$/AC. The peaks at 336.8 eV correspond to the Pd $3d_{5/2}$ electronic states of $Pd^{2+}$ species [36]. By calculating the integration areas of Pd° and $Pd^{2+}$ of Pd/@-$ZrO_2$/AC catalyst, it can be estimated that the percentage of Pd° and $Pd^{2+}$ were 69.6 % and 30.4 %, respectively. The percents were similar to those reported in the literature [37–39]. The results indicated that $Pd^{2+}$ could be reduced by photochemical route, the appearance of $Pd^{2+}$ species attributed to the electron transfer from Pd to $ZrO_2$ due to the strong interaction between Pd and $ZrO_2$ [33]. The Pd 3d spectra of Pd/$ZrO_2$ also shown in Fig. 1(e), the percentage of Pd° and $Pd^{2+}$ were 42.3 % and 57.7 %, respectively. Besides, Pd $3d_{5/2}$ for $Pd^{2+}$ was overlapped with Zr $3p_{3/2}$ in the XPS spectra, other researchers [33] also observed this phenomenon. The Zr 3d spectra was shown in Fig. 1(f), the peaks around 182.2 eV(Zr $3d_{5/2}$) and 184.5 eV(Zr $3d_{3/2}$) were assigned to the t-$ZrO_2$ [40].

The TEM and HRTEM images of $ZrO_2$/AC and Pd/@-$ZrO_2$/AC were shown in Fig. 2. For $ZrO_2$/AC(Fig. 2a and b), the m-$ZrO_2$ and t-$ZrO_2$ occurred simultaneously. It was supportive of the XRD observations. For Pd/@-$ZrO_2$/AC(Fig. 2d–f), the distance of 0.223 nm(measured crystal DigitalMicrograph) corresponding to the (111) plane of Pd. Meanwhile, energy-dispersive X-ray spectroscopy (EDS) mapping (Fig. 2g) confirmed the presence of elemental constituents with the as-synthesized samples and showed that Pd and Zr were uniformly distributed. Combined with Fig. 2a, it was difficult to distinguish the Pd nanoparticles and $ZrO_2$ from Fig. 2d, so Fig. 2c was the size distribution of Pd nanoparticles and $ZrO_2$, the average size was around 2.6 nm.

## 4. Hydrogenation of benzaldehyde

The activity of Pd-based catalysts for the hydrogenation of benzaldehyde was then investigated. For our purpose, we first investigated the effect of various solvents for the reaction. The corresponding conversion and selectivity list in Table 1 and the reaction pathways were shown in Scheme 2. When diethyl ether as a solvent, the benzaldehyde conversion was only 60.1 %, and a large amount of toluene (24.0 %) appeared in the product, the benzyl alcohol selectivity was only 70.3 %, and totally hydrogenation product methylcyclohexane (5.7 %) has appeared. The order of conversion of benzaldehyde→benzyl alcohol→toluene is predominant, while the formation of side ethers was actually inhibited, and (diethoxymethyl)benzene was not detected in the product. Methanol and ethanol gave a higher conversion but with a low selectivity toward benzyl alcohol. Because the benzaldehyde hydrogenation product benzyl alcohol contains hydroxyl groups, and methanol and ethanol also contained hydroxyl groups, they can be combined with each other in a hydrogen-bonding manner, so that the methoxy group and the ethoxy group participate in the reaction and generate (ethoxymethyl)benzene and anisole. These observations were also reported by several groups [7,16,41]. As we all know, the benzaldehyde and benzyl alcohol were soluble in diethyl ether, methanol and ethanol, and slightly soluble in water. When added benzaldehyde, benzyl alcohol and organic solvents in the autoclave, the mixture solution showed a single-phase, benzyl alcohol was not dissociation of the active site, so it was further hydrogenation for benzyl alcohol. When added benzaldehyde and benzyl alcohol in water, the mixture solution showed two phases, we conclude that the hydrogenation of benzaldehyde in water with the Pd/@-$ZrO_2$/AC catalyst may take place at the interface of aqueous and organic phases, inhibited the further hydrogenation of benzyl alcohol. Among the solvents tested, it seems that water has exhibited the highest activity(100%) and benzyl alcohol selectivity (98.1 %), and the use of water as a solvent complies with the rules of green chemistry.

The catalytic activities of these Pd catalysts in benzaldehyde hydrogenation were shown in Table 2. The $ZrO_2$/AC support (Table 2,

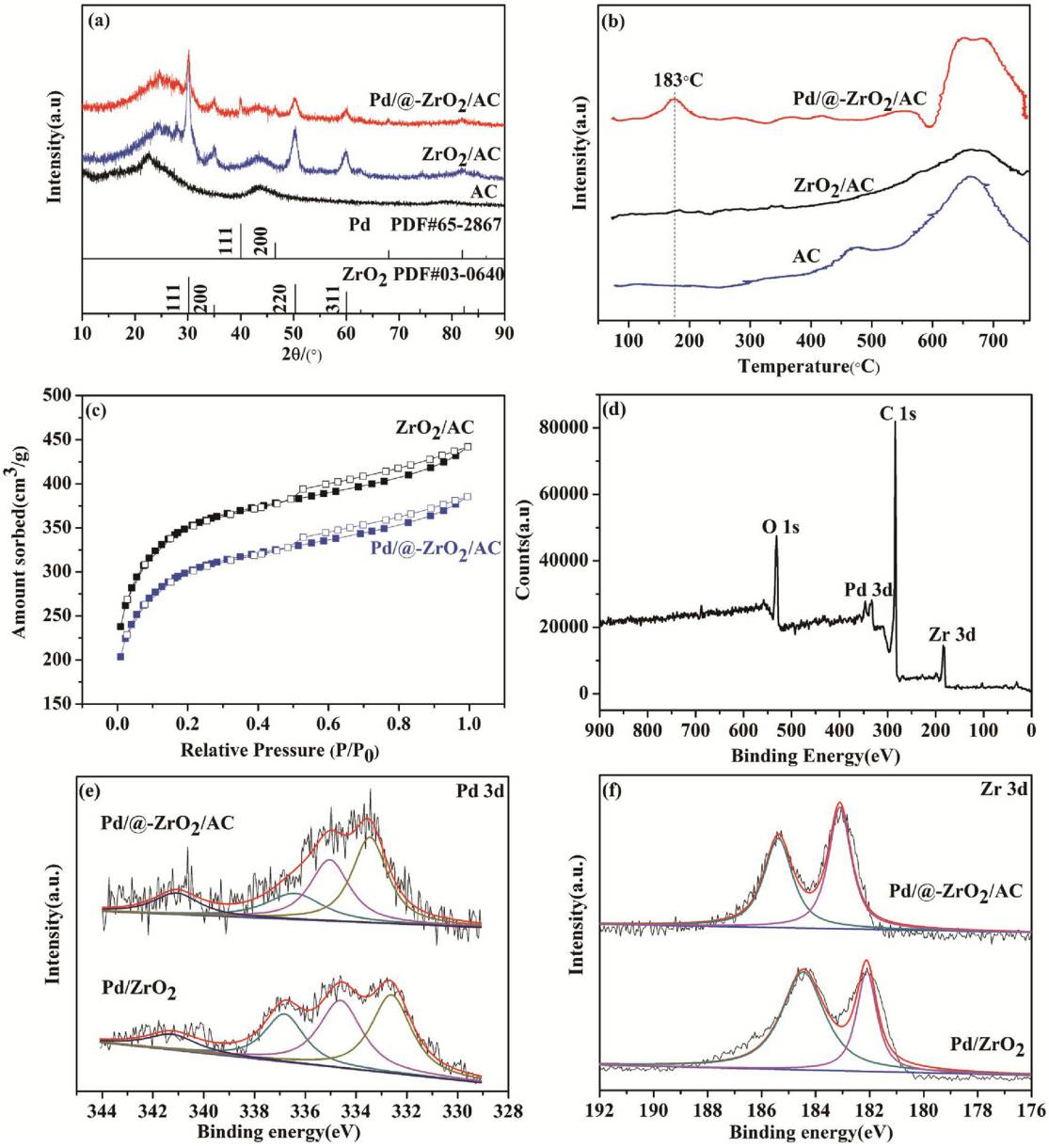


**Fig. 1.** XRD patterns (a) and $H_2$-TPR profiles (b) of Pd/@-$ZrO_2$/AC, $ZrO_2$/AC and AC; $N_2$ adsorption and desorption isotherms of Pd/@-$ZrO_2$/AC and $ZrO_2$/AC(c); survey XPS spectrum (d) and Pd 3d (e) Zr 3d (f) spectra of Pd/@-$ZrO_2$/AC and Pd/$ZrO_2$.

Entry 2) had no catalytic activity. Pd/$ZrO_2$ (Table 2, Entry 3) exhibited the lowest activity with a benzaldehyde conversion of 23.3 %, Pd/AC (Table 2, Entry 1) also gave an unsatisfactory conversion (29.7 %). It was interesting to note that Pd/@-$ZrO_2$/AC showed a remarkable conversion of 100% (Table 2, Entry 5) only within 30 min. Extended the reaction time to 60 min, the Pd/$ZrO_2$ and Pd/AC obtained 51.6 % and 70 % conversion, respectively, which was still lower than that of Pd/@-$ZrO_2$/AC. This result indicated that the activity was based on two major factors: (i) the special structure. The Pd/$ZrO_2$ and Pd/AC were the conventional catalysts which supported Pd on the support directly, this structure has been studied for many years in the selective hydrogenation, the activity was far from satisfactory, and thus researchers made the oxide into a special morphology to increase the surface area or added modifiers to improve the properties of the catalyst to improve the catalytic performance. Obviously, just because of the special structure of the Pd/@-$ZrO_2$/AC improved the activity, Pd supported on the $ZrO_2$/AC could produce novel materials, which not only take advantage of AC with a high surface area but also have the properties that the individual metal oxide does not have. (ii) The strong synergistic effect in the Pd/@-$ZrO_2$/AC catalyst. The turnover frequency(TOF, TOF = (Moles of reactant)/((load of Pt × m(cat.) × Pt dispersion/195.084) × (reaction time))) of Pd/@-$ZrO_2$/AC(16439 $h^{-1}$) was much higher than Pd/$ZrO_2$(6675 $h^{-1}$) and Pd/AC(7264 $h^{-1}$). This result indicated that there was a strong synergistic effect between metal nano-Pd and $ZrO_2$/AC.

When the Pd loading decreased to 0.8 % in Pd/@-$ZrO_2$/AC, 95.4 % conversion of benzaldehyde was achieved in water within 50 min (Table 2, Entry 8). When the Pd loading further decreased to 0.5 %, the catalyst attained 96.0 % conversion within 70 min (Table 2, Entry 10). Therefore, when decreased the loading of Pd, a high conversion of benzaldehyde can also be achieved by prolonging the reaction time.

To further understand the synergistic effect of this hybrid nanostructure catalyst, we investigated the hydrogenation of benzaldehyde over Pd/@-$Me_xO_y$/AC($Me_xO_y$: $TiO_2$, $CeO_2$, $La_2O_3$) catalysts. As can be seen, the activity of Pd/@-$Me_xO_y$/AC (Table 2, Entry 15, 18, 21) was higher than that of Pd/$Me_xO_y$ (Table 2, Entry 11–13). It indicated that

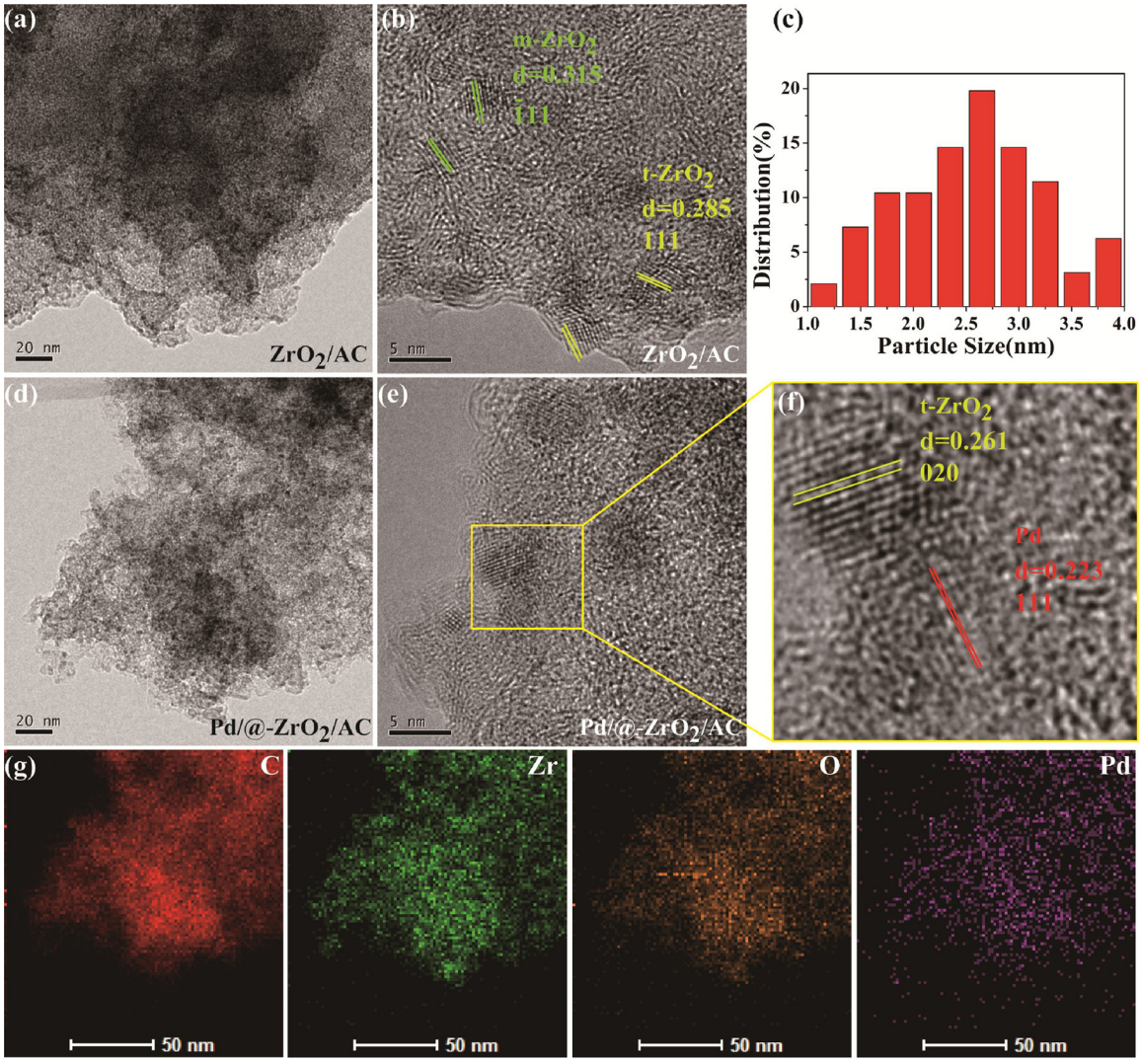


**Fig. 2.** TEM and HR-TEM images of $ZrO_2$/AC (a–b) and Pd/@-$ZrO_2$/AC (d–f); particle size distribution of Pd/@-$ZrO_2$/AC(e); an enlarged view of the portion containing Pd and $ZrO_2$ in Fig. 2e(f); EDS maps revealing that the Pd and the Zr elements are homogeneously distributed in Pd/@-$ZrO_2$/AC(g).

Pd supported on $Me_xO_y$/AC could form the hybrid nano-structure catalyst, which not only took advantage of the large specific surface area and pore volume of the carbon material but also had a property not possessed by a single metal oxide. The above results further confirmed the synergistic catalysis of these Pd/@-$Me_xO_y$/AC catalysts.

The content of metal oxide played an important role in the reaction. When the metal oxide content increased from 5 to 10 wt.% (Table 2, Entry 4–5, 14–15, 17–18, 20–21), the reaction went much faster. But increased the content of metal oxide from 10 to 15 wt.%, the conversion showed a downward trend. The group of Xie [30] reported that when the content of metal oxide was less than a certain threshold and surface area of the support was large enough, metal oxide would disperse on the support at the state of the spontaneous mono-layer distribution. When decreased the content of metal oxide, although the metal oxide was still dispersed on the AC at the state of the spontaneous mono-layer distribution, it was less than enough to cover the entire surface of the AC, the Pd/@-5 %$Me_xO_y$/AC consisted of major Pd/AC and slight Pd/@-$Me_xO_y$/AC. The structure of Pd/AC catalyst was supported Pd on the AC directly, this structure(metal/support) has been studied for many years, the activity was far from satisfactory. From Table 2, the Pd/AC only obtained 29.7 % conversion. When increased the content of the metal oxide to 15 wt.%, a small amount of metal oxide was dispersed on

**Table 1**
Hydrogenation of benzaldehyde over Pd/@-$ZrO_2$/AC catalyst by different solvents.

| Entry | Solvent | Conversion (%) | Selectivity(%)[a] | | | | |
|---|---|---|---|---|---|---|---|
| | | | BA | T | MC | DMB/EMB | A |
| 1 | $CH_3CH_2OCH_2CH_3$ | 60.1 | 70.3 | 24.0 | 5.7 | – | – |
| 2 | $CH_3OH$ | 83.9 | 21.9 | 33.7 | 12.6 | – | 31.8 |
| 3 | $CH_3CH_2OH$ | 99.4 | 5.8 | 71.5 | 7.1 | 15.6 | – |
| 4 | $H_2O$ | 100 | 98.1 | 1.9 | – | – | – |

Reaction conditions: catalyst(0.05 g), benzaldehyde(1.88 mmol), 30 min, 40°C, 0.7 MPa $H_2$ pressure, solvent(20 mL).
[a] Selectivity for benzyl alcohol(BA), toluene(T), methylcyclohexane(MC), (diethoxymethyl)benzene(DMB), (ethoxymethyl)benzene(EMB), anisole(A).

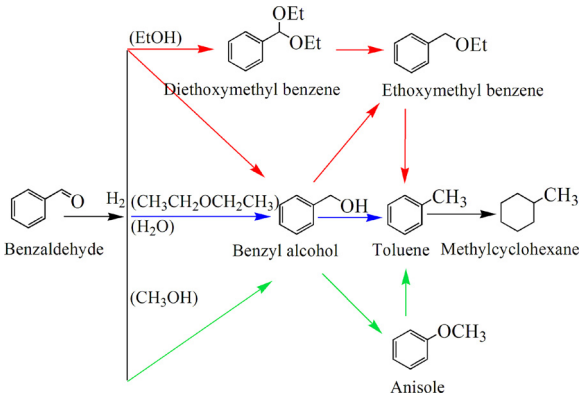


**Scheme 2.** Reaction pathways of benzaldehyde hydrogenation in different solvents.

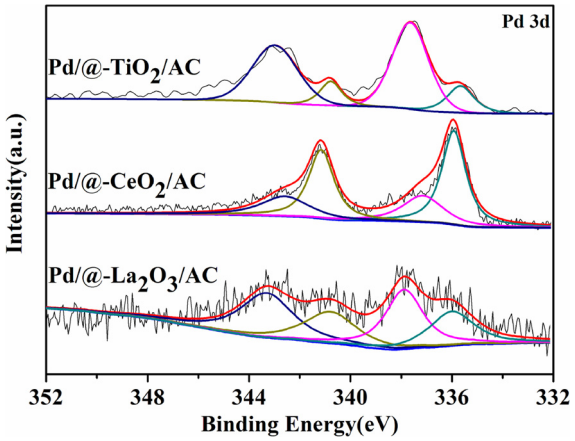


**Fig. 3.** Pd 3d spectra of Pd/@-$TiO_2$/AC, Pd/@-$CeO_2$/AC and Pd/@-$La_2O_3$/AC.

the AC at the state of the multilayer distribution, the surface area also decreased which might inhibit the adsorption of the reactants, resulting in a decrease in conversion.

In addition, Table 2 also revealed the difference in catalytic activity between Pd/@-$ZrO_2$/AC, Pd/@-$TiO_2$/AC, Pd/@-$CeO_2$/AC and Pd/@-$La_2O_3$/AC catalysts. The order of activity of the catalyst was Pd/@-$ZrO_2$/AC > Pd/@-$TiO_2$/AC > Pd/@-$La_2O_3$/AC > Pd/@-$CeO_2$/AC. The specific surface areas of Pd/@-$ZrO_2$/AC, Pd/@-$TiO_2$/AC, Pd/@-$La_2O_3$/AC and Pd/@-$CeO_2$/AC were 1162 $m^2$/g, 1188 $m^2$/g, 1368 $m^2$/g and 1245 $m^2$/g, respectively. This result indicated that it was not the higher the specific surface area, the higher the activity. Then we calculated the percentage of Pd° and $Pd^{2+}$ of these catalysts according to the XPS spectrum (Fig. 3, Table 3). It was known that the activation of hydrogen molecules was usually by the Pd°, the electron-deficient $Pd^{2+}$ species in the catalysts, which served as the electrophilic sites of adsorption and activation of the C═O bond in the benzaldehyde molecules [20]. From Table 3, these Pd catalysts with different metal oxide showed different electronic states of Pd. The Pd/@-$TiO_2$/AC had the highest percentage of $Pd^{2+}$ (69.1 %), which can be assigned to more electron transfer from Pd to $TiO_2$. Although a high percentage of $Pd^{2+}$ species adsorbed more benzaldehyde molecules, this didn't show high activity. Actually, the activation of hydrogen molecules or the

**Table 3**
Pd 3d XPS data and surface area of Pd/@-$TiO_2$/AC, Pd/@-$CeO_2$/AC and Pd/@-$La_2O_3$/AC.

| Sample | $Pd^0$(eV) | | $Pd^{2+}$(eV) | | $Pd^0/Pd^{2+}$(%) | Surface area ($m^2$/g) |
|---|---|---|---|---|---|---|
| Pd/@-$TiO_2$/AC | 340.8 | 335.7 | 343.1 | 337.8 | 30.8/69.1 | 1180 |
| Pd/@-$CeO_2$/AC | 341.1 | 336.0 | 342.8 | 337.1 | 67.1/32.9 | 1245 |
| Pd/@-$La_2O_3$/AC | 340.9 | 336.0 | 343.2 | 337.9 | 59.5/40.5 | 1368 |

**Table 2**
Hydrogenation of benzaldehyde over different catalysts.

| Entry | Catalyst | Time (min) | Conversion (%) | Selectivity(%)[a] | |
|---|---|---|---|---|---|
| | | | | BA | T |
| 1 | 1 %Pd/AC | 30 | 29.7 | 99.1 | 0.9 |
| 2 | 10 %$ZrO_2$/AC | 30 | – | – | – |
| 3 | 1 %Pd/$ZrO_2$ | 30 | 23.3 | 100 | 0 |
| 4 | 1 %Pd/@-5 %$ZrO_2$/AC | 30 | 44.6 | 99.2 | 0.8 |
| 5 | 1 %Pd/@-10 %$ZrO_2$/AC | 30 | 100 | 98.1 | 1.9 |
| 6 | 1 %Pd/@-15 %$ZrO_2$/AC | 30 | 95.0 | 98.3 | 1.7 |
| 7 | 0.8 %Pd/@-10 %$ZrO_2$/AC | 30 | 76.5 | 98.6 | 1.4 |
| 8 | 0.8 %Pd/@-10 %$ZrO_2$/AC | 50 | 95.4 | 98.8 | 1.2 |
| 9 | 0.5 %Pd/@-10 %$ZrO_2$/AC | 30 | 68.1 | 99.1 | 0.9 |
| 10 | 0.5 %Pd/@-10 %$ZrO_2$/AC | 70 | 96.0 | 98.4 | 1.6 |
| 11 | 1 %Pd/$TiO_2$ | 60 | 43.2 | 99.5 | 0.5 |
| 12 | 1 %Pd/$CeO_2$ | 60 | 55.6 | 99.7 | 0.3 |
| 13 | 1 %Pd/$La_2O_3$ | 60 | 49.0 | 100 | 0 |
| 14 | 1 %Pd/@-5 %$TiO_2$/AC | 60 | 38.1 | 100 | 0 |
| 15 | 1 %Pd/@-10 %$TiO_2$/AC | 60 | 95.9 | 98.0 | 2.0 |
| 16 | 1 %Pd/@-15 %$TiO_2$/AC | 60 | 80.1 | 98.3 | 1.7 |
| 17 | 1 %Pd/@-5 %$CeO_2$/AC | 60 | 50.5 | 99.1 | 0.9 |
| 18 | 1 %Pd/@-10 %$CeO_2$/AC | 60 | 87.3 | 98.6 | 1.4 |
| 19 | 1 %Pd/@-15 %$CeO_2$/AC | 60 | 82.1 | 98.8 | 1.2 |
| 20 | 1 %Pd/@-5 %$La_2O_3$/AC | 60 | 37.7 | 100 | 0 |
| 21 | 1 %Pd/@-10 %$La_2O_3$/AC | 60 | 89.4 | 99.4 | 0.6 |
| 22 | 1 %Pd/@-15 %$La_2O_3$/AC | 60 | 85.1 | 99.8 | 0.2 |
| 23[b] | 1 %Pd/@-10 %$ZrO_2$/AC | 30 | 42.0 | 100 | 0 |
| 24[b] | 1 %Pd/@-10 %$ZrO_2$/AC | 60 | 98.6 | 99.1 | 0.9 |
| 25 | 1 %Pd/CNTs | 30 | 87.2 | 99.5 | 0.5 |
| 26 | 1 %Pd/@-10 %$ZrO_2$/CNTs | 30 | 100 | 97.2 | 2.8 |

Reaction conditions: catalyst(0.05 g), benzaldehyde(1.88 mmol), 40°C, 0.7 MPa $H_2$ pressure, $H_2O$(20 mL).
[a] Selectivity for benzyl alcohol(BA), toluene(T).
[b] Second run to test the reusability of Pd/@-$ZrO_2$/AC.

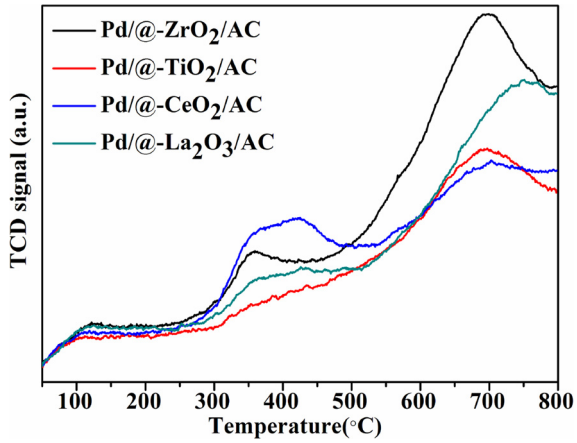


**Fig. 4.** The acidity properties of the Pd/@-$ZrO_2$/AC, Pd/@-$TiO_2$/AC, Pd/@-$CeO_2$/AC and Pd/@-$La_2O_3$/AC catalyst by $NH_3$-TPD.

adsorption of benzaldehyde molecules may be "just right" at some point of the relative ratio of the Pd species, so that the catalyst obtains the highest activity.

As we all know, the acidity of the catalyst may affect the catalytic activity, the $NH_3$-TPD (Fig. 4, Table 4) measurements were carried out to achieve the acidity of the Pd/@-$Me_xO_y$/AC catalysts. From Table 4, the total amount of acidity sites is in the order of Pd/@-$ZrO_2$/AC > Pd/@-$La_2O_3$/AC > Pd/@-$CeO_2$/AC > Pd/@-$TiO_2$/AC. Obviously, the acidity was not the major reason to influence the activity.

It has been reported that both the support and the surface metal atoms may be involved in determining the performance of catalysts [42]. Usually, the high dispersed noble metal catalyst often exhibits high catalytic performance. To learn more in-depth on the difference between the catalysts, the Pd/@-$Me_xO_y$/AC catalyst was characterized by TEM and HR-TEM (Fig. 5). As can be seen, it was difficult to distinguish the Pd nanoparticles and metal oxide from Figs. 2d and 5 a, e, i, so we gave the average particle sizes of Pd and metal oxide, the order was Pd/@-$ZrO_2$/AC(2.6 nm) < Pd/@-$TiO_2$/AC(3.4 nm) < Pd/@-$La_2O_3$/AC(8.7 nm) < Pd/@-$CeO_2$/AC(11.9 nm). According to the CO pulse chemisorption, the order of the Pd nanoparticle size was Pd/@-$ZrO_2$/AC(1.8 nm) < Pd/@-$TiO_2$/AC(2.3 nm) < Pd/@-$La_2O_3$/AC(4.3 nm) < Pd/@-$CeO_2$/AC(8.5 nm), the order of the Pt dispersion was Pd/@-$ZrO_2$/AC (61.0 %) > Pd/@-$TiO_2$/AC (49.4 %) > Pd/@-$La_2O_3$/AC (25.9 %) > Pd/@-$CeO_2$/AC (13.3%).

Table 2 shown that the order of activity of the catalyst was Pd/@-$ZrO_2$/AC > Pd/@-$TiO_2$/AC > Pd/@-$La_2O_3$/AC > Pd/@-$CeO_2$/AC. The above results demonstrated that the activity of this Pd catalysts was mainly affected by the particle size and Pt dispersion. The smaller the particle size, the higher Pt dispersion and the higher the activity.

After the reaction, the used catalyst was washed by deionized water (500 mL), then dried in a vacuum oven at 80°C for 10 h. We investigated the activity of the used Pd/@-$ZrO_2$/AC catalyst under the same reaction condition. The used catalyst only obtained 42.0 % conversion after the second cycle (Table 2, Entry 23), extended to 60 min, it obtained 98.6 % conversion and 99.1 % benzyl alcohol selectivity (Table 2, Entry 24). The Pd content of used Pd/@-$ZrO_2$/AC catalyst was about 0.9 wt.%, almost the same as that of the fresh Pd/@-$ZrO_2$/AC catalyst(0.92 wt.%). From Figure S1a, for the fresh and used catalyst, the weight losses occurred at 30-100°C, which was due to the desorption of physically absorbed water. For the used catalyst, a slight weight loss in the range of 150-300°C corresponded to the decomposition of organics. Combined with $N_2$ adsorption-desorption analysis, the specific surface area of catalyst was reduced from 1162 $m^2$/g to 925 $m^2$/g and pore volume is decreased from 0.6 to 0.5 $cm^3$/g. TEM images of fresh and used catalysts were shown in Figure S2(a–b). Compared with fresh catalyst, the Pd nanoparticles of used Pd/@-$ZrO_2$/AC catalyst was obviously agglomerated. This result indicates that the reason for the deactivation could be mainly ascribed to the pore blockage with organic matters including benzaldehyde and benzyl alcohol, and the agglomeration of Pd nanoparticles.

**Table 4**
The acidic properties of the Pd/@-$ZrO_2$/AC catalyst by $NH_3$-TPD.

| Catalyst | 250-500°C | | > 500°C | | Total $n_{NH3}$ (μmol/g) |
|---|---|---|---|---|---|
| | Peak temperature (°C) | $n_{NH3}$ (μmol/g) | Peak temperature (°C) | $n_{NH3}$ (μmol/g) | |
| Pd/@-$ZrO_2$/AC | 361.8 | 793.4 | 696.8 | 2863.5 | 3656.9 |
| Pd/@-$TiO_2$/AC | 425.7 | 713.5 | 750.9 | 1962.7 | 2676.2 |
| Pd/@-$CeO_2$/AC | 423.6 | 1112.1 | 703.0 | 1633.5 | 2745.6 |
| Pd/@-$La_2O_3$/AC | 424.5 | 726.3 | 696.8 | 2330.9 | 3057.2 |

According to the literature report [43,44], the support with regular pore structure may maintain the structure of the catalyst to keep its stability, so we used the CNTs as support to investigate the stability of this hybrid nano-structure Pd catalyst, obtained Pd/@-$ZrO_2$/CNTs catalyst. This catalyst also exhibited synergistic catalysis, the order of the activity was Pd/@-$ZrO_2$/CNTs(100%) > Pd/CNTs(87.2%) > Pd/$ZrO_2$ (23.3%)(40°C, 30 min, 0.7 MPa). The result of catalytic hydrogenation of benzaldehyde was shown in Fig. 6. To our delight, the catalyst showed no distinct loss in activity or selectivity after second time cycles. When the catalyst was subjected to the fifth cycles, it still maintained a higher activity (62 %) than that of Pd/$ZrO_2$ (23.3 %). Although this Pd/@-$ZrO_2$/CNTs catalyst can avoid organic blocking pores(Figure S1b, Figure S3), Pd nanoparticles still aggregated after five cycles (Figure S2c-d). These results indicate that in order to avoid structural changes or pore-clogging after multiple reuses of the catalyst, it is necessary to develop a catalyst for immobilizing Pd nanoparticles on a support having a regular pore structure and a high degree of stability for the process. Based on the above discussion, whether AC or CNTs as a carrier, these hybrid nano-structure catalysts can exhibit a synergistic effect, and we believe our strategy offers an attractive opportunity for selectivity hydrogenation.

## 5. Conclusions

In summary, a hybrid nano-structure Pd/@-$ZrO_2$/AC catalyst has been prepared by a photochemical route. This catalyst exhibited high activity(100% conversion, > 98% selectivity) for the hydrogenation of benzaldehyde to benzyl alcohol at 40°C using water as a clean solvent. The high catalytic performance was attributed to the special structure of the catalyst, and the synergistic effect between Pd nanoparticles and $ZrO_2$/AC, which leads to a well-dispersed of Pd coated on the $ZrO_2$/AC surface. And the Pd/@-$TiO_2$/AC, Pd/@-$CeO_2$/AC, and Pd/-$La_2O_3$/AC catalysts further confirmed the synergistic effect in this hybrid nano-structure for this reaction. After the second cycle, the Pd/@-$ZrO_2$/AC catalyst obtained 98.6 % conversion and 99.1 % benzyl alcohol selectivity at 40°C when extended the reaction time to 60 min. When using CNTs as a support, the Pd/@-$ZrO_2$/CNTs catalyst showed no distinct loss in activity (98 % conversion) or selectivity (100%) after second time cycles at 40°C within 30 min. Thus, the combination of nano-metals and nano-semiconductors/porous materials forms a hybrid nano-structure catalyst with synergistic effects that are expected to be used in a series of selective hydrogenation of heterogeneously catalyzed reactions.

## Acknowledgements

This work was supported by the Natural Science Foundation of China (21676227), the Key Project of Hunan Provincial Natural Science Foundation of China (09JJ3021).

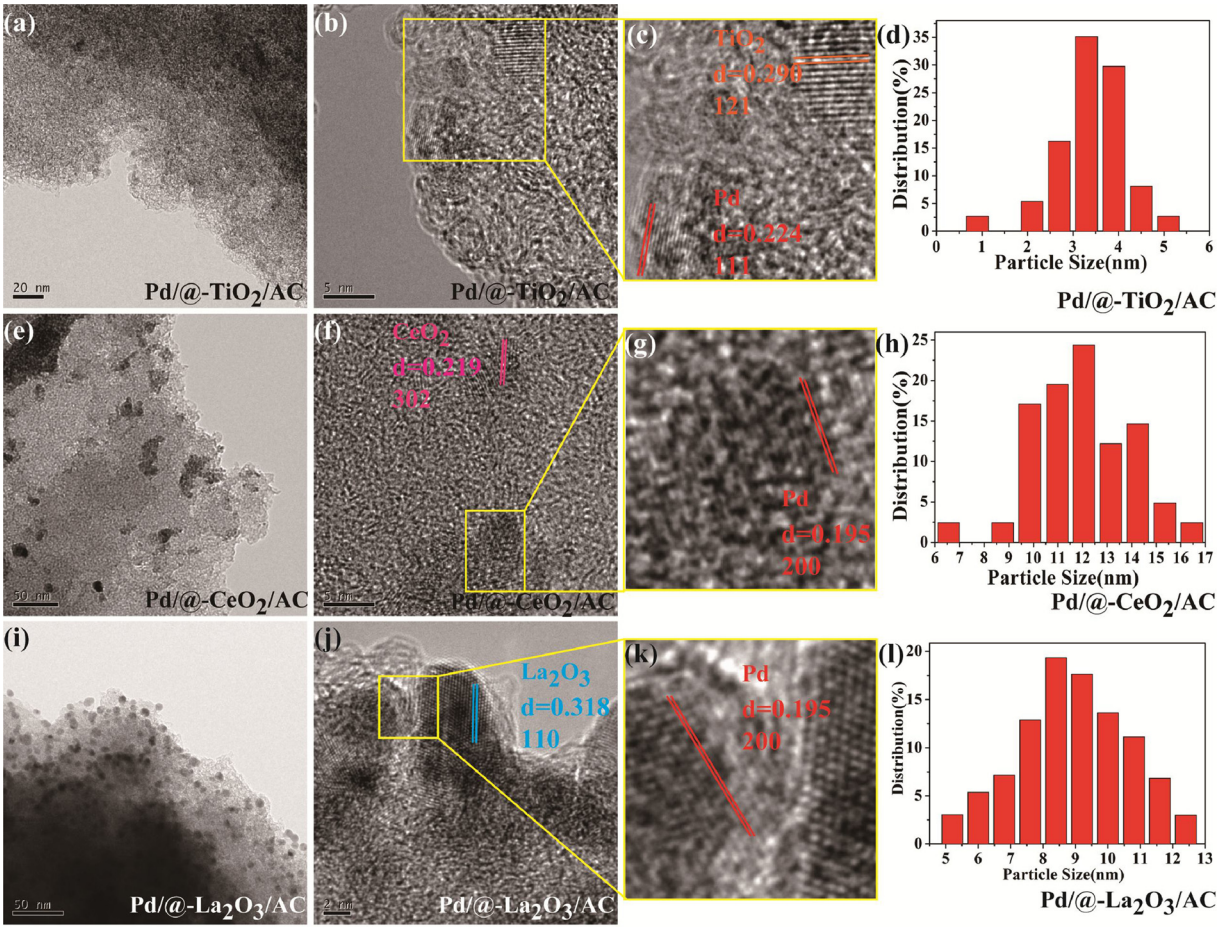


**Fig. 5.** TEM and HR-TEM images and particle size distributions of Pd/@-$TiO_2$/AC (a–d); Pd/@-$CeO_2$/AC (e–h); Pd/@-$La_2O_3$/AC (i–l).

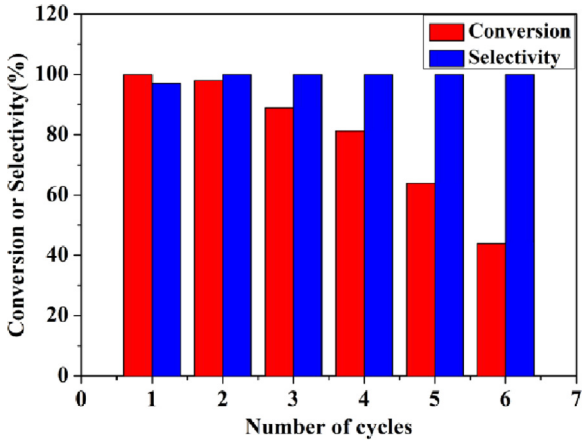


**Fig. 6.** Reusability of the Pd/@-$ZrO_2$/CNTs catalyst toward the hydrogenation of benzaldehyde. Reaction conditions: catalyst(0.05 g), benzaldehyde (1.88 mmol), 30 min, 40°C, 0.7 MPa $H_2$ pressure, $H_2O$(20 ml).

## Appendix A. Supplementary data

Supplementary material related to this article can be found, in the online version, at doi:https://doi.org/10.1016/j.cattod.2020.01.022.

## References

[1] T.B. Jayesh, K. Itika, G.V. Ramesh Babu, K.S. Rama Rao, R.S. Keri, Arvind H. Jadhav, B.M. Nagaraja, Vapour phase selective hydrogenation of benzaldehyde to benzyl alcohol using Cu supported Mg-Al hydrotalicite catalyst, Catal. Commun. 106 (2018) 73–77.

[2] M. Han, H. Zhang, Y. Du, P. Yang, Z. Deng, Catalytic hydrogenation of benzaldehydes over platinum nanoparticles immobilized on magnesium aluminate spinel under mild conditions, React. Kinet. Mech. Cat. 102 (2011) 393–404.

[3] F. Yan, C. Zhao, L. Yi, J. Zhang, B. Ge, T. Zhang, W. Li, Effect of the degree of dispersion of Pt over $MgAl_2O_4$ on the catalytic hydrogenation of benzaldehyde, J. Catal. 38 (2017) 1613–1620.

[4] D. Divakar, D. Manikandan, G. Kalidoss, T. Sivakumar, Hydrogenation of benzaldehyde over palladium intercalated bentonite catalysts: kinetic studies, Catal. Lett. 125 (2008) 277–282.

[5] N. Perret, F. Cárdenas-Lizana, M.A. Keane, Selective hydrogenation of benzaldehyde to benzyl alcohol over Au/$Al_2O_3$, Catal. Commun. 16 (2011) 159–164.

[6] N. Haddada, A. Saadi, A. Löfberg, R.N. Vannier, E. Bordes-Richard, C. Rabia, Benzaldehyde reduction over Cu-Al-O bimetallic oxide catalyst. Influence of pH during hydrothermal synthesis on the structural andcatalytic properties, J. Mol. Catal. A-Chem. 396 (2015) 207–215.

[7] P. Liu, Y. Zhao, R. Qin, S. Mo, G. Chen, L. Gu, D.M. Chevrier, P. Zhang, Q. Guo, D. Zang, B. Wu, G. Fu, N. Zheng, Photochemical route for synthesizing atomically dispersed palladium catalysts, Science 352 (2016) 797–800.

[8] F. Pinna, F. Menegazzo, M. Signoretto, P. Canton, G. Fagherazzi, N. Pernicone, Consecutive hydrogenation of benzaldehyde over Pd catalysts influence of supports and sulfur poisoning, Appl. Catal. A-Gen. 219 (2001) 195–200.

[9] A. Saadi, R. Merabti, Z. Rassoul, M.M. Bettahar, Benzaldehyde hydrogenation over supported nickel catalysts, J. Mol. Catal, A-Chem. 253 (2006) 79–85.

[10] A. Saadi, K. Lanasri, K. Bachari, D. Halliche, C. Rabia, Catalytic reduction of benzaldehyde under hydrogen flow over nickel-containing mesoporous silica catalysts, Open J. Phys. Chem. 2 (2012) 73–80.

[11] Y. Song, U. Sanyal, D. Pangotra, J.D. Holladay, D.M. Camaioni, O.Y. Gutiérrez, J.A. Lercher, Hydrogenation of benzaldehyde via electrocatalysis and thermal catalysis on carbon-supported metals, J. Catal. 359 (2018) 68–75.

[12] A. Saadi, Z. Rassoul, M.M. Bettahar, Gas phase hydrogenation of benzaldehyde over supported copper catalysts, J. Mol. Catal, A-Chem. 164 (2000) 205–216.

[13] X. Kong, L. Chen, Chemoselective hydrogenation of aromatic aldehydes over $SiO_2$ modified Co/γ-$Al_2O_3$, Appl. Catal. A-Gen. 476 (2014) 34–38.

[14] H. Pan, X. Li, Y. Yu, J. Li, J. Hu, Y. Guan, P. Wu, Pt nanoparticles entrapped in mesoporous metal-organic frameworks MIL-101 as an efficient catalyst for liquid-phase hydrogenation of benzaldehydes and nitrobenzenes, J. Mol. Catal, A-Chem. 399 (2015) 1–9.

[15] Y. Ding, X. Li, B. Li, H. Wang, P. Wu, Pt nanoparticles entrapped in ordered

mesoporous carbons for liquid-phase hydrogenation of unsaturated compounds, Catal. Commun. 28 (2012) 147–151.
[16] X. Li, W. Zheng, H. Pan, Y. Yu, L. Chen, P. Wu, Pt nanoparticles supported on highly dispersed $TiO_2$ coated on SBA-15 as an efficient and recyclable catalyst for liquid-phase hydrogenation, J. Catal. 300 (2013) 9–19.
[17] F. Zhao, S. Fujita, A.S. Akihara, M. Arai, Hydrogenation of benzaldehyde and cinnamaldehyde in compressed $CO_2$ medium with a Pt/C catalyst: a study on molecular interactions and pressure effects, J. Phys. Chem. A 19 (2005) 4419–4424.
[18] M. Li, X. Wang, F. Cárdenas-Lizana, M.A. Keane, Effect of support redox character on catalytic performance in the gas phase hydrogenation of benzaldehyde and nitrobenzene over supported gold, Catal. Today 279 (2017) 19–28.
[19] M. Li, X. Wang, N. Perret, M.A. Keane, Enhanced production of benzyl alcohol in the gas phase continuous hydrogenation of benzaldehyde over $Au/Al_2O_3$, Catal. Commun. 46 (2014) 187–191.
[20] R.M. Mironenkoa, O.B. Belskaya, T.I. Gulyaeva, M.V. Trenikhin, A.I. Nizovskii, A.V. Kalinkin, V.I. Bukhtiyarov, A.V. Lavrenov, V.A. Likholobov, Liquid-phase hydrogenation of benzaldehyde over Pd-Ru/C catalysts: synergistic effect between supported metals, Catal. Today 279 (2017) 2–9.
[21] Y. Ding, X. Li, H. Pan, P. Wu, Ru nanoparticles entrapped in ordered mesoporous carbons: an efficient and reusable catalyst for liquid-phase hydrogenation, Catal. Lett. 144 (2014) 268–277.
[22] Y. Gao, S. Jaenicke, G.K. Chuah, Highly efficient transfer hydrogenation of aldehydes and ketones using potassium formate over AlO(OH)-entrapped ruthenium catalysts, Appl. Catal. A-Gen. 484 (2014) 51–58.
[23] J.A. Lopez-Ruiz, U. Sanyal, J. Egbert, O.Y. Gutiérrez, J. Holladay, Kinetic investigation of the sustainable electrocatalytic hydrogenation of benzaldehyde on Pd/C: effect of electrolyte composition and half-cell potentials, ACS Sustain. Chem. Eng. 6 (2018) 16073–16085.
[24] Y. Zhou, J. Liu, X. Li, X. Pan, X. Bao, Selectivity modulation in the consecutive hydrogenation of benzaldehyde via functionalization of carbon nanotubes, J. Nat. Gas Chem. 21 (2012) 241–245.
[25] X. Guo, D. Jang, H. Jang, G. Kim, Hydrogenation and dehydrogenation reactions catalyzed by CNTs supported palladium catalysts, Catal. Today 186 (2012) 109–114.
[26] A. Proto, R. Cucciniello, A. Genga, C. Capacchione, A study on the catalytic hydrogenation of aldehydes using mayenite as active support for palladium, Catal. Commun. 68 (2015) 41–45.
[27] M. Okamoto, T. Hirao, T. Yamaai, Polymers as novel modifiers for supported metal catalyst in hydrogenation of benzaldehydes, J. Catal. 276 (2010) 423–428.
[28] T. Osako, K. Torii, S. Hirata, Y. Uozumi, Chemoselective continuous-flow hydrogenation of aldehydes catalyzed by platinum nanoparticles dispersed in an amphiphilic resin, ACS Catal. 7 (2017) 7371–7377.
[29] R. Radhakrishan, D.M. Do, S. Jaenicke, Y. Sasson, G.K. Chuah, Potassium phosphate as a solid base catalyst for the catalytic transfer hydrogenation of aldehydes and ketones, ACS Catal. 1 (2011) 1631–1636.
[30] J.Q. Si, W.B. Ouyang, Y.J. Zhang, W.T. Xu, J.C. Zhou, Novel nano-semiconductor film layer supported nano-Pd complex nanostructured catalyst Pd/℗-MeOx/AC for high efficient selective hydrogenation of phenol to cyclohexanone, Sci. Rep. U. K. 7 (2017) 1254.
[31] Y.J. Zhang, J.C. Zhou, J.Q. Si, Synergistic catalysis of nano-Pd and nano rareearth oxide/AC: complex nanostructured catalysts fabricated by a photochemical route for selective hydrogenation of phenol, RSC Adv. 7 (2017) 54779–54788.
[32] Y. Xie, Y. Tang, Spontaneous monolayer dispersion of oxides and salts onto surfaces of supports: applications to heterogeneous catalysis, Adv. Catal. 37 (1990) 1–43.
[33] Z. Shao, H. Xu, H. Wan, F. Chen, L. Liu, S. Li, Zheng, Influence of $ZrO_2$ properties on catalytic hydrodechlorination of chlorobenzene over $Pd/ZrO_2$ catalysts, J. Hazard. Mater. 179 (2010) 135–140.
[34] Y. Yuan, Z. Wang, H. An, W. Xue, Y. Wang, Oxidative carbonylation of phenol with a $Pd\text{-}O/CeO_2$-nanotube catalyst, Chin. J. Catal. 36 (2015) 1142–1154.
[35] W. Yu, H.W. Lin, C.S. Tan, Direct synthesis of Pd incorporated in mesoporous silica for solvent-free selective hydrogenation of chloronitrobenzenes, Chem. Eng. J. 325 (2017) 124–133.
[36] M. Guo, H. Li, Y.Q. Ren, X.M. Ren, Q.H. Yang, C. Li, Improving catalytic hydrogenation performance of Pd nanoparticles by electronic modulation using phosphine ligands, ACS Catal. 8 (2018) 6476–6485.
[37] T.Z. Liu, H. Zhou, B.B. Han, Y.B. Gu, S.Q. Li, J. Zheng, X. Zhong, G.L. Zhuang, J.G. Wang, Enhanced selectivity of phenol hydrogenation in low-pressure $CO_2$ over supported Pd catalysts, ACS Sustain. Chem. Eng. 5 (2017) 11628–11636.
[38] Y. Wang, J. Yao, H.R. Li, D.S. Su, M. Antonietti, Highly selective hydrogenation of phenol and derivatives over a Pd@Carbon nitride catalyst in aqueous media, J. Am. Chem. Soc. 133 (2011) 2362–2365.
[39] G.Y. Xu, J.H. Guo, Y. Zhang, Y. Fu, J.Z. Chen, L.L. Ma, Q.X. Guo, Selective hydrogenation of phenol to cyclohexanone over Pd-HAP catalyst in aqueous media, ChemCatChem 7 (2015) 2485–2492.
[40] S.R. Ginjupalli, S. Mugawar, P. Rajan N, P.K. Balla, V.R. Chary Komandur, Vapour phase dehydration of glycerol to acrolein over tungstated zirconia catalysts, Appl. Surf. Sci. 309 (2014) 153–159.
[41] M. Shirai, O. Sato, N. Hiyoshi, A. Yamaguchi, Enhancement of reaction rates for catalytic benzaldehyde hydrogenation and sorbitol dehydration in water solvent by addition of carbon dioxide, J. Chem. Sci. 2 (2014) 395–401.
[42] W. Du, S. Xia, R. Nie, Z. Hou, Magnetic Pt catalyst for selective hydrogenation of Halonitrobenzenes, Ind. Eng. Chem. Res. 53 (2014) 4589–4594.
[43] Y.H. Zhou, Qh. Yang, Y.Z. Chen, H.L. Jiang, Low-cost CuNi@MIL-101 as an excellent catalyst toward cascade reaction: integration of ammonia borane dehydrogenation with nitroarene hydrogenation, Chem. Commun. 53 (2017) 12361–12364.
[44] F. Li, R. Ma, B. Cao, J.R. Liang, Q.M. Ren, H. Song, Effect of Co-B supporting methods on the hydrogenation ofm-chloronitrobenzene over Co-B/CNTs amorphous alloy catalysts, Appl. Catal. A Gen. 514 (2016) 248–252.